

# SABRE polarized low field rare-spin spectroscopy

Cite as: J. Chem. Phys. **152**, 184202 (2020); <https://doi.org/10.1063/5.0002412>

Submitted: 24 January 2020 . Accepted: 15 April 2020 . Published Online: 13 May 2020

Sören Lehmkühl , Martin Suefke , Arne Kentner, Yi-Fen Yen , Bernhard Blümich , Matthew S. Rosen , Stephan Appelt , and Thomas Theis 



View Online



Export Citation



CrossMark

Lock-in Amplifiers  
up to 600 MHz



# SABRE polarized low field rare-spin spectroscopy

Cite as: *J. Chem. Phys.* **152**, 184202 (2020); doi: 10.1063/5.0002412

Submitted: 24 January 2020 • Accepted: 15 April 2020 •

Published Online: 13 May 2020



Sören Lehmkuhl,<sup>1,a)</sup> Martin Siefert,<sup>2</sup> Arne Kentner,<sup>3</sup> Yi-Fen Yen,<sup>4</sup> Bernhard Blümich,<sup>3</sup>   
Matthew S. Rosen,<sup>4,5</sup> Stephan Appelt,<sup>2,3,6</sup> and Thomas Theis<sup>1,7,a)</sup>

## AFFILIATIONS

<sup>1</sup>Department of Chemistry, North Carolina State University, 851 Main Campus Dr, Raleigh, North Carolina 27606, USA

<sup>2</sup>Institute of Energy and Climate Research (IEK-9), Forschungszentrum Jülich GmbH, 52425 Jülich, Germany

<sup>3</sup>Institute of Technical and Macromolecular Chemistry, RWTH Aachen University, Worringerweg 2, 52056 Aachen, Germany

<sup>4</sup>Martinos Center for Biomedical Imaging, Massachusetts General Hospital, Boston, Massachusetts 02129, USA

<sup>5</sup>Department of Physics, Harvard University, Cambridge, Massachusetts 02138, USA

<sup>6</sup>Central Institute for Engineering, Electronics and Analytics – Electronic Systems (ZEA-2), Forschungszentrum Jülich GmbH, 52425 Jülich, Germany

<sup>7</sup>Joint Department of Biomedical Engineering, University of North Carolina at Chapel Hill and North Carolina State University, Raleigh, North Carolina 27695, USA

**Note:** This paper is part of the JCP Special Topic on Spin Chemistry.

<sup>a)</sup> **Authors to whom correspondence should be addressed:** [slehmku@ncsu.edu](mailto:slehmku@ncsu.edu) and [ttheis@ncsu.edu](mailto:ttheis@ncsu.edu)

## ABSTRACT

High-field nuclear magnetic resonance (NMR) spectroscopy is an indispensable technique for identification and characterization of chemicals and biomolecular structures. In the vast majority of NMR experiments, nuclear spin polarization arises from thermalization in multi-Tesla magnetic fields produced by superconducting magnets. In contrast, NMR instruments operating at low magnetic fields are emerging as a compact, inexpensive, and highly accessible alternative but suffer from low thermal polarization at a low field strength and consequently a low signal. However, certain hyperpolarization techniques create high polarization levels on target molecules independent of magnetic fields, giving low-field NMR a significant sensitivity boost. In this study, SABRE (Signal Amplification By Reversible Exchange) was combined with high homogeneity electromagnets operating at mT fields, enabling high resolution <sup>1</sup>H, <sup>13</sup>C, <sup>15</sup>N, and <sup>19</sup>F spectra to be detected with a single scan at magnetic fields between 1 mT and 10 mT. Chemical specificity is attained at mT magnetic fields with complex, highly resolved spectra. Most spectra are in the strong coupling regime where *J*-couplings are on the order of chemical shift differences. The spectra and the hyperpolarization spin dynamics are simulated with SPINACH. The simulations start from the parahydrogen singlet in the bound complex and include both chemical exchange and spin evolution at these mT fields. The simulations qualitatively match the experimental spectra and are used to identify the spin order terms formed during mT SABRE. The combination of low field NMR instruments with SABRE polarization results in sensitive measurements, even for rare spins with low gyromagnetic ratios at low magnetic fields.

Published under license by AIP Publishing. <https://doi.org/10.1063/5.0002412>

## I. INTRODUCTION

Nuclear magnetic resonance (NMR) spectroscopy has emerged as a valuable tool for the characterization of chemical compounds as NMR spectra of virtually all compounds containing spin-1/2 nuclei can be readily obtained on a commercial spectrometer. Indeed, NMR has advanced to one of the most useful techniques for chemical and structural identification.<sup>1–6</sup> Generally, large superconducting high-field (>1 T) magnets are used to generate the strong,

homogeneous magnetic fields needed to obtain high-resolution NMR spectra. These high-field superconducting magnets require controlled access laboratory facilities to mitigate the potential hazards of these magnetic fields. In contrast, NMR instruments operating at very low magnetic fields can be made more compact, accessible, and less expensive than their high field brethren. There are many examples of sensitive setups that perform NMR in the magnetic field of the Earth, at zero field, or in the milliTesla (mT) regime.<sup>7–16</sup> Operation at a low magnetic field, in general, affects

instrument sensitivity, and one strategy to boost sensitivity is to use passive and active high- $Q$  external resonators,<sup>17,18</sup> but the largest experimental limitation to the widespread use of these devices comes from the intrinsically low Boltzmann spin polarization at a low field. Hyperpolarization techniques that can be used to create high nuclear spin polarization independent of the magnetic field are a promising enabling solution at a low field.

Popular hyperpolarization methods include dynamic nuclear polarization (DNP),<sup>19–21</sup> spin-exchange optical pumping (SEOP),<sup>22–24</sup> and chemically induced DNP (CIDNP).<sup>25,26</sup> A particularly simple hyperpolarization approach is parahydrogen induced polarization (PHIP). PHIP was first introduced by Bowers and Weitkamp.<sup>27,28</sup> More recently, Signal Amplification By Reversible Exchange (SABRE)<sup>29</sup> has emerged as a more generalizable variant of PHIP that allows for hyperpolarization on many classes of compounds. SABRE uses a transition-metal catalyst to transfer spin order from parahydrogen through a transient  $J$ -coupling network on the catalyst to target molecules. When polarizing protons, this spin-order transfer is most efficient at magnetic fields of order several mT as has been demonstrated in various studies.<sup>30–33</sup> This can be understood by the concept of level anti-crossings (LACs).<sup>34–37</sup> A further extension of this technique known as SABRE-SHEATH (SABRE in SHield Enables Alignment Transfer to Heteronuclei)<sup>38,39</sup> can generate magnetization on heteronuclei by polarization-transfer fields in the  $\mu$ T regime. The detection of heteronuclei is important for many applications, especially for biochemical and structural characterizations,<sup>1</sup> and indeed, by using hyperpolarization, low concentrated analytes can be detected at low magnetic fields.<sup>40–42</sup>

In the present work, we demonstrate the unique utility of combining low-field NMR instruments with SABRE hyperpolarization to enable chemically specific spectroscopy of  $^1\text{H}$  and rare spins, including  $^{15}\text{N}$ ,  $^{13}\text{C}$ , and  $^{19}\text{F}$ . We demonstrate experimental results obtained from a low-field electromagnet-based spectroscopy system with an external high-quality ( $Q$ ) resonator and from a low-field electromagnet-based MRI scanner operating at 6.5 mT. We compare the experimental spectra to simulations obtained with

a modified version of the SPINACH code<sup>43</sup> in an attempt to understand the underlying mechanism involving the hyperpolarization chemistry and the spin-physics in the polarization-transfer complexes. With the simulations, we qualitatively match the experimental spectra and identify the spin order terms formed during mT SABRE. We describe a surprisingly pronounced magnetic field dependence on the structure of the spectra in a range of 1–10 mT. The methods and spectroscopy equipment used here are described, followed by a demonstration of experimental low-field spectra of SABRE polarized molecules containing rare spins, and finally simulations with corresponding spin dynamics to explain and rationalize our observations.

## II. METHODS

This section is subdivided into three parts. In Sec. II A, we describe the experimental setups, including the low-field spectroscopy electromagnet with the external high- $Q$  resonator (EHQE),<sup>17</sup> the low-field electromagnet-based MRI scanner (without EHQE),<sup>44</sup> the setup for parahydrogen production and delivery, and the data processing. In Sec. II B, we describe the hyperpolarization chemistry, i.e., preparation and measurement of the SABRE samples. In Sec. II C, we elaborate on the simulations of the NMR spectra, which was performed in MATLAB with the SPINACH software from the Kuprov Lab<sup>43</sup> with custom modifications.

### A. Experimental setup

NMR spectra were obtained from two different electromagnet-based low-field systems. The first system is a high homogeneity spectroscopy magnet [Fig. 1(a)] uses a hand-wound cylindrical copper coil with 10 mm diameter [Fig. 1(b)] coupled to an external ferrite resonator (EHQE). This low-field setup and its EHQE-NMR detection approach are described in detail by Suefke *et al.*<sup>17</sup> The  $B_0$  field for detection is created by a cylindrical coil made of copper wire and can be shimmed to a homogeneity below 1 ppm for a sensitive

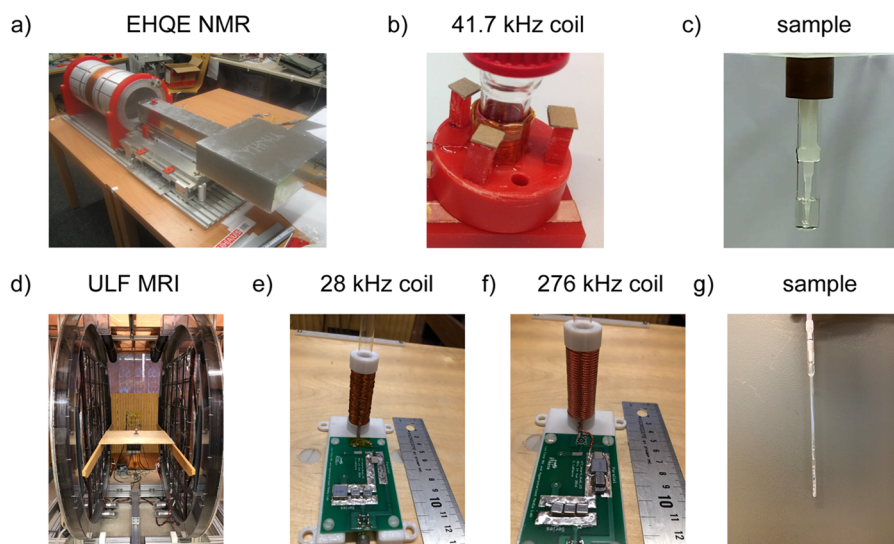


**FIG. 1.** Setup of the spectroscopy electromagnet [(a)–(c)] and the 6.5 mT ultra-low field (ULF) MRI scanner [(d)–(g)]: (a) electromagnet with an EHQE resonator, (b) 41.7 kHz detection coil, (c) parahydrogen bubbling through the SABRE active solution using a pipette tip and a small glass vial, (d) imaging magnet with the detection coil in the middle, (e) coil for 28 kHz ( $^1\text{H}$ ) detection at 6.5 mT, (f) coil for 276 kHz ( $^{15}\text{N}$ ) detection at 6.5 mT, and (g) parahydrogen bubbling through a SABRE active solution with Teflon tubing in a high-pressure NMR tube.

volume of 500  $\mu\text{l}$ . The signal is detected with a solenoid coil matched to 41.7 kHz and coupled to a ferrite core to obtain a high  $Q$  factor [ $Q \sim 200\text{--}400$ , Figs. 1(a) and 1(b)]. After preamplification, the signal is fed into a lock-in amplifier and recorded at a rate of 16 kHz (16 bit resolution) at an off-resonance frequency of about 60 Hz. For all nuclei ( $^1\text{H}$ ,  $^{19}\text{F}$ ,  $^{13}\text{C}$ , and  $^{15}\text{N}$ ), the resonance frequency was kept the same (41.7 kHz) by adjusting the magnetic field strength, i.e., 1 mT for  $^1\text{H}$ , 1.1 mT for  $^{19}\text{F}$ , 4 mT for  $^{13}\text{C}$ , and 10 mT for  $^{15}\text{N}$ . For these experiments, the Bruker Parahydrogen Generator (BPG) was employed, yielding approximately 85% parahydrogen fraction. The raw data were zero filled, Fourier transformed, and first-order phase corrected by using custom-made python software. The amplitude of the signal is given in arbitrary units (a.u.) but matches for all experiments of a given compound. Notice that even amplitudes from different nuclei in the same compound are directly comparable because only the magnetic field was changed and the signals were received with the same coil at the same frequency.

The second low-field instrument is the ultra-low field (ULF) MRI scanner [Fig. 1(d)] described by Sarracanie *et al.*<sup>44</sup> This system is a state-of-the-art custom-made 6.5 mT (276 kHz  $^1\text{H}$  frequency) biplanar electromagnet-based scanner with homogeneity better than 0.25 Hz over a 10 mm NMR sample tube and equipped with 3 axis imaging gradients (1 mT/m). A multi-nuclear Tecmag Redstone spectroscopy and imaging console, with nine Rx channels and three Tx channels, drives the system. RF transmit is provided by Tomco power amplifiers (BT00500-AlphaS for  $^1\text{H}$  and BT00250-AlphaA for  $^{15}\text{N}$ ), and MITEQ low-noise preamps (AU-1583 for  $^1\text{H}$  at 276 kHz and AU-1442 for  $^{15}\text{N}$  at 28 kHz) are used. For the experiments described here, the scanner was operated with a field-frequency lock that provides immunity to time-varying environmental fields of better than 0.25 Hz/day.

For the work described here, a  $^1\text{H}$  coil tuned to 276 kHz [Fig. 1(e)] and a  $^{15}\text{N}$  coil tuned to 28 kHz [Fig. 1(f)] were constructed with a 10 mm ID. Parahydrogen was enriched at liquid nitrogen temperature, yielding  $\sim 51\%$  fractional parahydrogen content. Spectra were acquired with  $90^\circ$  pulses using a four step phase cycle.

In all experiments (except SABRE-SHEATH), the hyperpolarization field ( $B_{\text{evo}}$ ) and the detection field are identical, i.e., the samples are exposed to parahydrogen via bubbling in the detection field. Only one experiment is different, where we hyperpolarized  $^{15}\text{N}$ -acetonitrile in a  $\mu$ -metal shield (SABRE-SHEATH)<sup>45</sup> and transferred to 10 mT for detection.

## B. Hyperpolarization chemistry and sample preparation

Samples were prepared using Schlenk techniques in an inert gas atmosphere and kept under inert conditions during experiments. The chemicals (Sigma Aldrich) were dried with a molecular sieve and degassed before use. The catalyst precursor [IrCl(cod)IMes] [cod = cyclooctadiene, IMes = 1,3-bis(2,4,6-trimethylphenyl)imidazole-2-ylidene] was synthesized from [Ir(cod)(OMe)]<sub>2</sub> and 2 equivalents of IMes·HCl in acetone and recrystallized three times in methanol for purification. The samples contained 1.5  $\mu\text{l}$  of the to-be-polarized substrate and 1.76 mg catalyst precursor in 900  $\mu\text{l}$  methanol-*d*<sub>4</sub>, unless otherwise stated. In the case of acetonitrile as a substrate, 7.5  $\mu\text{l}$  acetonitrile were used, and 3  $\mu\text{l}$  pyridine-*d*<sub>5</sub> were added to stabilize the catalytic complex.

Parahydrogen was bubbled through the solution for 15 min to activate the catalyst. During this time, the yellow color of the solution faded [see Figs. 1(c) and 1(f)]. The parahydrogen was supplied through PTFE tubing submerged in the SABRE-active solution [Fig. 1(b)]. The susceptibility artifacts at such low detection fields caused by the polystyrene pipette tip (spectroscopy magnet) or the PTFE capillary (imaging magnet) and the gaseous parahydrogen are negligible. Thus, parahydrogen was constantly bubbled through the solution during measurements.

SABRE-SHEATH experiments were conducted in a  $\mu$ -metal shield, which attenuates the earth's magnetic field. The required  $B_{\text{evo}}$  is generated by a small coil inside this shield allowing for ultra-low fields between 0.1  $\mu\text{T}$  and 500  $\mu\text{T}$ .

## C. Simulations

The NMR spectra were simulated in MATLAB (R2019a) using the SPINACH software 2.3.4934 from the Kuprov Lab<sup>43</sup> and modified, as described below. The simulations were compared to measurements at 41.7 kHz, 276 kHz, and 28 kHz. In addition, the SABRE-SHEATH experiment was simulated by including field-cycling.

We explored two simulation approaches. In the first approach, referred to as the “quick” method, we simply guessed the spin order created on the molecules during SABRE and simulated the spectra until a match was obtained. This “quick” approach yields good agreement between simulation and experiment, and the simulations were fast (of the order seconds). In the second approach, which we term “complete,” we simulated the hyperpolarization transfer process starting from the parahydrogen singlet state on the polarization transfer complex. While this “complete” approach helps to understand the polarization transfer mechanism, it is far more cumbersome to obtain a match between experiment and simulation, and the simulations take longer, tens of minutes to a few hours on a desktop computer, making iterations toward experiment–simulation match tedious. Nonetheless, we were able to achieve qualitative agreement and explain the underlying mechanisms.

In the “complete” approach, the simulations needed to take into account the underlying chemistry as well as the spin evolution at the low magnetic fields used in the experiments. The simulated spin system consists of the nuclei of the target molecule as well as the two parahydrogen derived hydrides. From the  $J$ -couplings and chemical shifts of these spins, the Hamiltonian was formulated. The parameters used to simulate the individual spin systems were taken from the literature and are listed in the [supplementary material](#).<sup>46,47</sup> In some cases, we also had to adjust the  $J$ -coupling values to achieve agreement with the experiments. In particular, the sign of the  $J$ -couplings is often ambiguous in the literature; however, the relative signs of the  $J$ -couplings have large effects on the simulated spectra. Full details are discussed in the [supplementary material](#). In brief, the initial density matrix was a singlet between the two hydride protons in the bound hyperpolarization complex. This density matrix was evolved under the Hamiltonian of the complex at the specified magnetic field. The resulting evolution was weighted exponentially by the exchange rate (details below) and averaged. Then, the hydrides were decoupled from the spin system, leaving behind the free substrate in the solution. The resulting density matrix on the substrate was evolved for an additional 10 s (sufficiently long to

allow for reliable averaging) under the Hamiltonian of the substrate and averaged. Finally, a  $90^\circ$  pulse was applied, and the spectrum was calculated.

To simulate the exchanging nature of the SABRE system, we consider that the supply of parahydrogen is the rate determining step due to either the speed of the oxidative addition or the diffusion limited supply and replacement of hydrogen with parahydrogen in solution. This goes hand-in-hand with the experimental observations that the signal increases with increasing parahydrogen pressure and flow rates.<sup>10,33,38,40,48,49</sup> For the simulations, the consequence is that we neglected the possibility of hydride exchange during hyperpolarization events and solely focused on substrate exchange. This implies that once a parahydrogen molecule is bound to iridium, the efficiency of polarization transfer depends on the rate of substrate exchange. For the classical pyridine case, an optimum substrate exchange rate of  $\sim 4.5\text{ s}^{-1}$  has been predicted theoretically<sup>50</sup> and confirmed experimentally.<sup>51</sup> Strategies for optimizations of other SABRE substrates include adding another ligand<sup>52</sup> or changing the temperature,<sup>48</sup> which bring the substrate exchange rate into the desired regime. To simulate the effects of exchange, the density matrix, starting from the hydride singlet, was evolved for 1 s in time steps of 0.1 ms obtaining 10 000 different density matrices. To take into account the probability of dissociation, an exponential decay with a decay constant  $k$  is applied to the density matrices, and then, they are averaged. An average lifetime of 40 ms was assumed for the pyridine and 3-fluoropyridine complex and a 30 ms lifetime for the acetonitrile complex. Subsequently, the two hydride protons are decoupled from the spin system leaving the free, dissociated substrate behind. Then, the density matrix of the free substrate is further evolved for 10 s. Specifically, the density matrix is calculated for 10 000 time steps of 1 ms. The amount of each obtained spin state should depend on its relaxation time. Thus, these density matrices were again weighted with an exponential weighting function accounting for the relaxation time of  $\sim 1.0$  s. Finally, all the density matrices are summed up and read out after applying a  $90^\circ$  pulse, concluding the “complete” approach.

For both the “quick” and “complete” approaches, a line broadening ( $\text{lb}$ ) representing the average linewidth of the individual experiments was chosen according to the inhomogeneities of the different instruments. The simulated FIDs were zero-filled 4 times the detection time, Fourier-transformed, and plotted. We provide both simulation approaches, “quick” and “complete,” for all the studied molecules. In the [supplementary material](#), we provide examples of the SPINACH MATLAB code for both “quick” and “complete” simulations.

### III. RESULTS AND DISCUSSION

Low-field NMR spectra of several compounds containing different rare spin labels were studied. They include  $^{13}\text{C}$ ,  $^{15}\text{N}$ , and  $^{19}\text{F}$  in the form of  $^{13}\text{C}$ -acetonitrile,  $^{15}\text{N}$ -pyridine,  $^{15}\text{N}$ -acetonitrile, and 3-fluoropyridine. The observed spectra differ significantly from their unlabeled analogs (which typically give a single line) because adding an additional spin  $1/2$  nucleus with a different  $\gamma$  to a spin system breaks the magnetic equivalence of the protons at a low field. This results in information-rich spectra that elucidate the SABRE dynamics, when the spectra are compared to simulations.

#### A. $^{13}\text{C}$ -acetonitrile

As a first molecule, acetonitrile is examined. Its spin system gives NMR spectra that are simpler and easier to interpret. Two isotopomers of acetonitrile were studied:  $^{13}\text{C}$ -acetonitrile and  $^{15}\text{N}$ -acetonitrile. For the  $^{13}\text{C}$ -acetonitrile, we chose  $\text{CH}_3^{13}\text{CN}$  (instead of  $^{13}\text{CH}_3\text{CN}$ ) because of the higher  $^{13}\text{C}$  polarization under the chosen SABRE conditions.<sup>53</sup> The structure, the resulting  $^1\text{H}$  spectrum, and the  $^{13}\text{C}$  spectrum are shown in [Fig. 2](#). The proton spectrum of the  $^{13}\text{C}$ -acetonitrile acquired at 1 mT features an antiphase doublet with a coupling constant of  $^2J_{\text{CH}} = 10.3\text{ Hz}$  [[Fig. 2\(a\)](#)]. The simulated spectrum [[Fig. 2\(c\)](#)], using the “quick” simulation approach, matches the experimental spectrum. For this simulation, a sum of longitudinal, two-spin order (typical for SABRE experiments<sup>53</sup>), and four-spin order was chosen for consistency with the  $^{15}\text{N}$ -acetonitrile experiment, as detailed below. We note that two-spin order alone also gives a spectrum consistent with the  $^1\text{H}$  experiment, however, not with the  $^{15}\text{N}$  spectra, as discussed below. The [supplementary material](#) provides the simulated  $^{15}\text{N}$  spectra starting from the individual spin orders (one-, two-, three-, and four-spin orders) to clearly illustrate their individual contributions.

The  $^{13}\text{C}$  spectrum, acquired at 4 mT (41.7 kHz), is a quartet with the same coupling constant [[Fig. 2\(b\)](#)]. Remarkably, this 4 mT carbon spectrum is fully in phase, and its signal-to-noise ratio ( $\sim$ polarization) is considerably lower. These observations can be rationalized because the polarization-transfer field (4 mT) does not match proton or carbon level anti-crossings well, leading to poor polarization transfer. The small detected  $^{13}\text{C}$  polarization likely stems from NOE effects/cross relaxation from the proton polarization. To account for this observation in the simulation, only  $I_z$  spin order on the  $^{13}\text{C}$  was included in the initial state in the “quick” approach [see [Fig. 2\(d\)](#)].

#### B. $^{15}\text{N}$ -acetonitrile

In  $^{15}\text{N}$ -acetonitrile, the coupling to the protons is significantly lower than in the carbon case  $^3J_{\text{NH}} = 1.74\text{ Hz}$  (instead of 10.3 Hz to  $^{13}\text{C}$ ). Apart from that, the proton spectrum looks identical in shape; it is an antiphase doublet indicating longitudinal, heteronuclear two-spin order [[Fig. 3\(a\)](#)]. The corresponding “quick” simulation is depicted in [Fig. 3\(d\)](#). The coupling of the  $^{15}\text{N}$  to the hydrides, in contrast to  $^{13}\text{C}$ , is considerably stronger. This allows for a higher polarization transfer to the  $^{15}\text{N}$  heteronucleus. The  $^{15}\text{N}$  polarization was created using two different polarization transfer fields: the detection field  $B_0$  of 10 mT and a  $2\text{ }\mu\text{T}$  SABRE-SHEATH field. The quartet in the  $^{15}\text{N}$  spectra ( $^3J_{\text{NH}} = 1.74\text{ Hz}$ ) has antiphase character when transfer occurs at  $B_0 = 10\text{ mT}$  (41.7 kHz  $^{15}\text{N}$  frequency) with relative intensities  $(-1; -2; +2; +1)$ , indicating 2-spin or higher even-spin ordered terms [see [Fig. 3\(b\)](#)]. Therefore, the “quick” simulation uses an initial state of two- and four-spin order  $I_z(1)S_z(4) + I_z(2)S_z(4) + I_z(3)S_z(4) - 2I_z(1)I_z(2)I_z(3)S_z(4)$  [[Fig. 3\(e\)](#)], as shown by Sufke *et al.*<sup>17</sup> The [supplementary material](#) details how the initial spin order is identified for the “quick” simulations and provides full details for the “complete” simulation. The complete simulation gives an inverted intensity distribution of  $(-1; -2; +1; +2)$ . This was already shown in the first publication of acetonitrile polarization by Mewis *et al.*,<sup>53</sup> where the intensities also did not match, but two of them were switched.

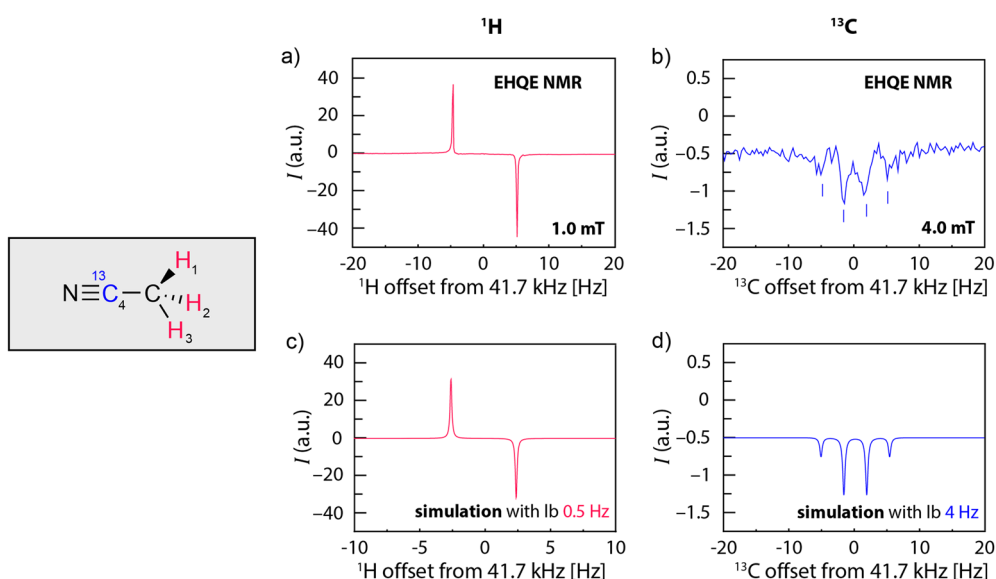


**FIG. 2.**  $^{13}\text{C}$ -labeled acetonitrile: (a)  $^1\text{H}$  spectrum of acetonitrile at 41.7 kHz labeled with  $^{13}\text{C}$  at the nitrile carbon, (b) corresponding  $^{13}\text{C}$  spectrum at 41.7 kHz, (c) “quick” simulation of the proton spectrum starting from  $I_z(1)\mathbf{S}_z(4) + I_z(2)\mathbf{S}_z(4) + I_z(3)\mathbf{S}_z(4) - 2I_z(1)I_z(2)I_z(3)\mathbf{S}_z(4)$ , and (d) “quick” simulation of the carbon spectrum with starting state  $\mathbf{S}_z(4)$  after suggested cross relaxation/NOE.  $^2J_{\text{CH}} = 10.3$  Hz. The spin order for the  $^1\text{H}$  spectrum simulated with the “quick” approach is chosen as is for consistency with the  $^{15}\text{N}$  labeled acetonitrile experiments, even though all the individual terms yield the same spectrum (see the  $^1\text{H}$  spectrum of  $^{15}\text{N}$  acetonitrile in the [supplementary material](#)). The “complete” simulations are provided in the [supplementary material](#) as well.

More polarization is obtained in the SHEATH experiment [Fig. 3(c)]. The SABRE-SHEATH<sup>4</sup> experiment utilizes  $\mu\text{T}$  transfer fields to allow for more efficient polarization transfer to heteronuclei. For the corresponding “quick” simulation [Fig. 3(f)], we used  $I_z$  spin order created by SABRE-SHEATH and LAC at the  $\mu\text{T}$  field. The “complete” simulation is shown in the [supplementary material](#) and matches the experimental spectrum.

### C. Pyridine

Next, we discuss the most common SABRE target, pyridine. At high fields, pyridine produces readily interpretable spectra; however, spectra in the strong coupling regime, at low magnetic fields, differ from high-field spectra. The low-field spectrum of  $^{15}\text{N}$ -pyridine is rather complicated.<sup>54</sup> In Fig. 4, such spectra are shown at 41.7 kHz for  $^1\text{H}$  and  $^{15}\text{N}$  of  $^{15}\text{N}$ -pyridine. The signal created by the hyperpolarization is so intense that recorded FIDs can be recorded for many seconds, resulting in highly resolved, yet complicated peak patterns. In contrast to the acetonitrile spectrum, where molecular couplings could be directly extracted, this more complicated  $^{15}\text{N}$ -pyridine spectrum could be used for structure identification based on its fingerprint instead. One possible approach to such specificity could be a database that matches the obtained spectra with reference spectra as done in mass spectrometry. Nonetheless, we note that  $J$ -couplings as well as nonlinearly included chemical shift differences can, in principle, be extracted from such spectra as has been demonstrated already.<sup>12</sup> Alternatively, the spectra can be compared to a simulation as we do here. For the  $^1\text{H}$  spectrum of  $^{15}\text{N}$ -pyridine, the simulation qualitatively matches the

experimental spectrum, when the individual SABRE polarization levels of the *ortho*-, *meta*-, and *para*-protons are considered as has been shown previously.<sup>54</sup> A similar “quick” simulation using Spinach is shown in the [supplementary material](#) for comparison (comparable agreement is obtained). Here, shown in Fig. 4(c), the simulation uses the “complete” approach starting with a singlet state of the hydrides. The simulation accounts for the different evolution times on the catalyst depending on complex lifetime, as well as evolution of the free pyridine after dissociation, limited by relaxation. In this way, a spectrum is simulated that displays matching line positions and similar intensities. Small deviations can originate from sources such as other catalytic intermediates during SABRE, different or multiple binding mechanisms, the solvent (methanol) as well as counterion ( $\text{Cl}^-$ ) binding to the catalyst, uncertainties in small  $J$ -couplings, and exchange of parahydrogen at the catalytic center.<sup>55</sup> Despite these uncertainties, the match between experiment and simulation is good.

The  $^{15}\text{N}$  experiment was recorded at a 10 times higher field than  $^1\text{H}$  to obtain the same acquisition frequency (41.7 kHz). The signal is significantly lower than for  $^1\text{H}$  as the LAC for  $^{15}\text{N}$  is far away [Fig. 4(b)]. In the spectrum, the lines from the coupling of  $^{15}\text{N}$  to all the different protons can be identified. The spectrum was also simulated using the “complete” approach in analogy to the  $^1\text{H}$  experiment [Fig. 3(d)]. The line positions and signs match but are represented slightly better with a “quick” simulation starting with an initial spin-order guess, as shown in the [supplementary material](#).

To demonstrate the generality of rare spin spectroscopy with SABRE, the same system was investigated in the human-scale 6.5 mT

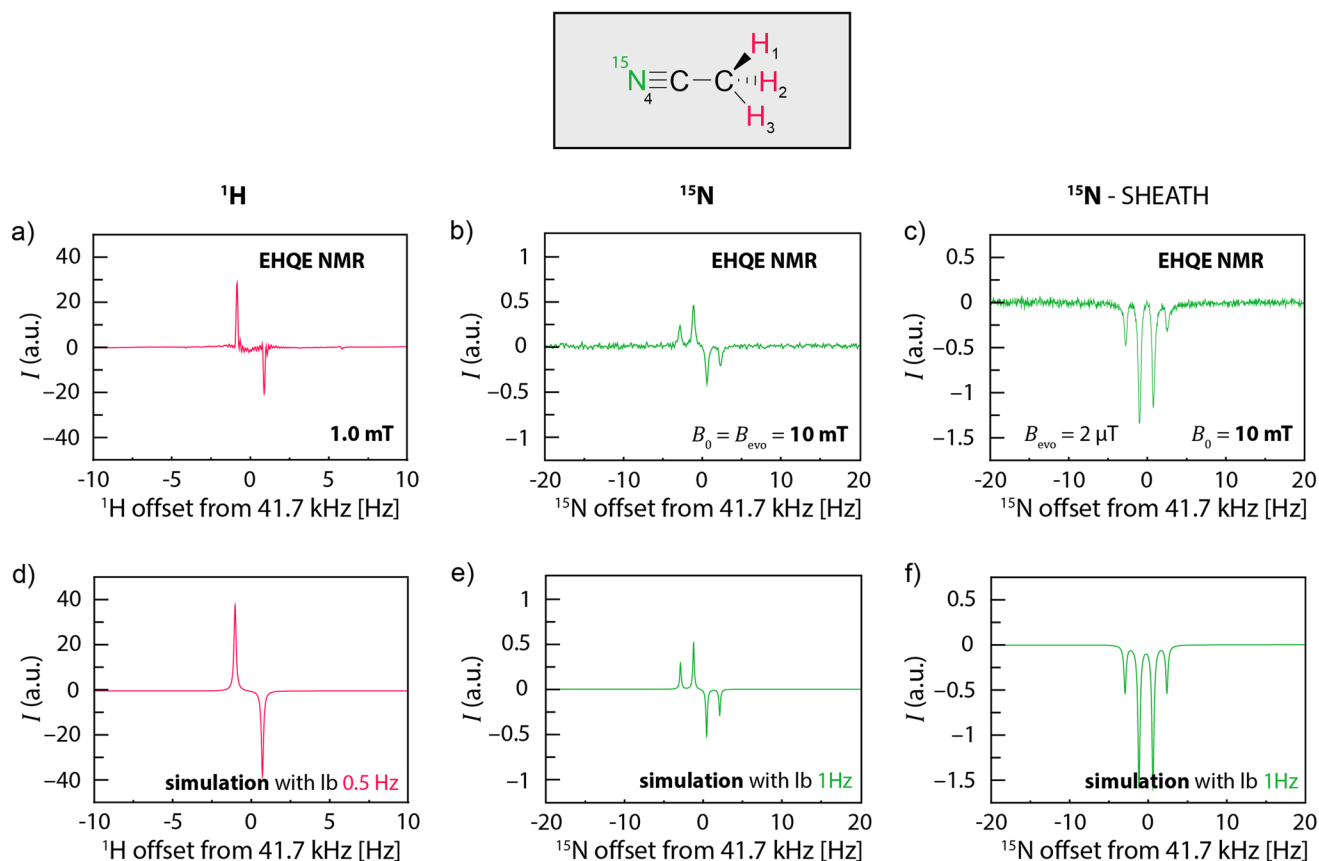


**FIG. 3.**  $^{15}\text{N}$ -labeled acetonitrile with  $J_{\text{NH}} = 1.74$  Hz: (a)  $^1\text{H}$  spectrum at 41.7 kHz, (b) corresponding  $^{15}\text{N}$  spectrum at 41.7 kHz, and (c)  $^{15}\text{N}$  SABRE-SHEATH experiment: shuttling from the  $2\ \mu\text{T}$  field for polarization into 10 mT for detection. [(d)–(f)] “Quick” simulations with the initial state for (d) and (e)  $I_z(1)\mathbf{S}_z(4) + I_z(2)\mathbf{S}_z(4) + I_z(3)\mathbf{S}_z(4) - 2I_z(1)I_z(2)I_z(3)\mathbf{S}_z(4)$ , only single spin order  $\mathbf{S}_z(4)$  for (f) (“complete” simulations provided in the [supplementary material](#)).

ULF MRI scanner instead of the EHQE NMR system. At 6.5 mT, the polarization transfer to protons is more efficient.<sup>30–33</sup> Despite its higher detection field, the setup is slightly less sensitive due to the absence of EHQE, slightly reduced homogeneity, and use of only 50% parahydrogen. Nonetheless, well resolved rare-spin spectra are obtained. In this magnet, the field was constant at 6.5 mT, and the frequency was varied from 276 kHz for  $^1\text{H}$  to 28 kHz for  $^{15}\text{N}$ . The proton spectrum shows in-phase peaks from pyridine as well as broad peaks with the opposite phase at around 20 Hz off-resonance to the hydrides in the bound complex. The spectrum of free pyridine [Fig. 4(g)] was simulated in the same way as Fig. 4(c). Its shape could be reproduced when accounting for the broader linewidth in the less homogeneous imaging magnet. A narrower linewidth was also simulated, showing more lines expected in a more homogeneous magnet (shown in light red). The measured and simulated  $^{15}\text{N}$  spectra in the ULF MRI magnet (at 6.5 mT) are very similar to the ones in the solenoid magnet setup (at 10 mT), except for slightly lower signal-to-noise ratio (SNR) and slightly wider lines.

#### D. 3-fluoropyridine

SABRE polarization of  $^{19}\text{F}$  on 3-fluoropyridine has already been demonstrated in the original report<sup>29</sup> and has been studied in more detail by Shchepin *et al.*<sup>56</sup> In the first report, no spectroscopic information, i.e.,  $J$ -coupling, was observed. Recently, superconducting quantum interference device (SQUID) based low-field NMR was used to study SABRE polarized 3-fluoropyridine.<sup>57</sup> Buckenmaier *et al.* thoroughly studied hyperpolarized homo- and heteronuclear higher order spin states of this molecule and selected multi-quantum coherences by phase cycling in modified COSY experiments at  $\mu\text{T}$  fields. Here, in the homogeneous low field at 41 kHz, well resolved  $J$ -coupling information is obtained. The proton spectrum [Fig. 5(a)] features a complicated manifold of lines due to the coupling of the four inequivalent protons to  $^{19}\text{F}$  as well as the homonuclear  $^1\text{H}$  couplings in the strong coupling regime. In order to achieve a matching simulation all  $J$ -couplings in the molecule are critical. In the  $^{19}\text{F}$  spectrum [Fig. 5(b)], 16 doublets from the couplings to the protons in the weak coupling regime can be identified. The antiphase nature

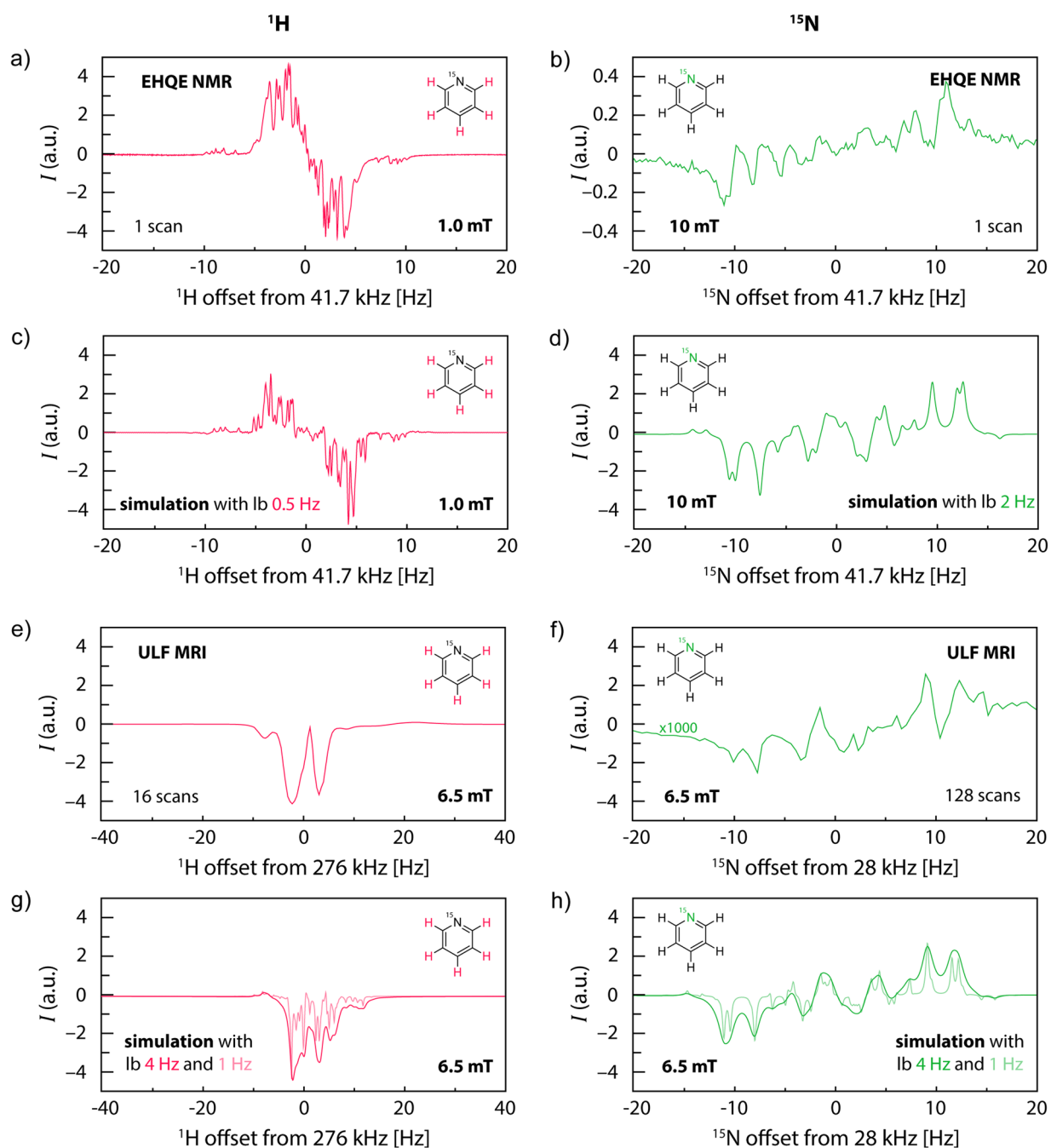


**FIG. 4.**  $^1\text{H}$  and  $^{15}\text{N}$  low-field spectra of  $^{15}\text{N}$ -pyridine: [(a) and (b)] single-scan SABRE spectra recorded at 41.7 kHz on the solenoid electromagnet (EHQE NMR), [(c) and (d)] corresponding “complete” simulations accounting for the spin evolution and the chemical dynamics, [(e) and (f)]  $^1\text{H}$  and  $^{15}\text{N}$  spectra of  $^{15}\text{N}$ -pyridine recorded in the ULF MRI magnet at 6.5 mT, and [(g) and (h)] corresponding “complete” simulations accounting for the spin evolution and the chemical dynamics (“quick” simulations provided in the [supplementary material](#)).

suggests two-spin or higher even ordered spin terms. In the proton spectrum, the contribution of higher spin-order terms is minor (around 10%, see the [supplementary material](#)), and the main polarization stems from coherent spin mixing at the LAC for pyridine

and its derivatives. The simulations [Figs. 5(c) and 5(d)] use the “complete” approach starting from the parahydrogen singlet. The corresponding “quick” simulations, which use a guessed initial spin order to produce a good match, are shown in the [supplementary material](#).

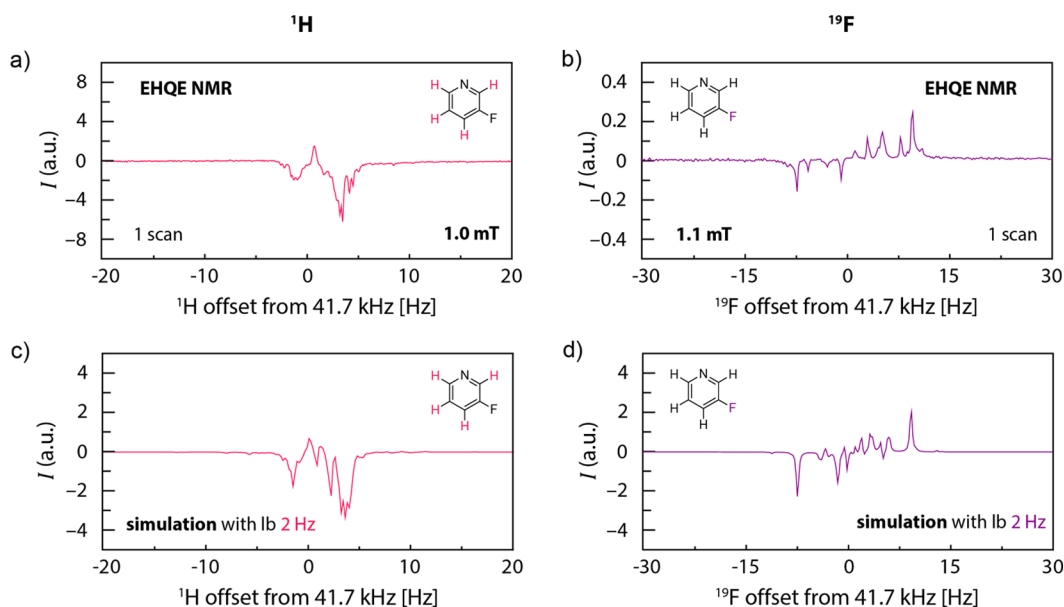


**FIG. 5.** Low-field SABRE spectra of 3-fluoropyridine at 41.7 kHz: [(a) and (b)] scan  $^1\text{H}$  and  $^{19}\text{F}$  spectra recorded on the solenoid electromagnet and [(c) and (d)] corresponding “complete” simulations accounting for the spin evolution and the chemical dynamics (“quick” simulations provided in the [supplementary material](#)).

#### IV. CONCLUSION AND OUTLOOK

High-resolution low-field NMR was combined with SABRE hyperpolarization. This combination produces a very sensitive measurement technique to give high resolution spectra.  $^1\text{H}$ ,  $^{13}\text{C}$ ,  $^{15}\text{N}$ , and  $^{19}\text{F}$  spectra at low magnetic fields were recorded with spectroscopic resolution. It is also possible to execute such experiments in less homogeneous fields of imaging magnets without external high quality factor enhancement (EHQE), still providing highly resolved spectra and sufficient SNR, as shown for  $^{15}\text{N}$ -pyridine. The spectra feature more information than standard high-field spectra in the weak coupling regime but are more difficult to interpret. The spectra for all compounds are compared to simulations. Two simulation approaches for SPINACH are introduced, which yield good agreement with the observed spectra. The “quick” approach, where initial states are guessed for the SABRE polarized substrates, typically gives better agreement with the experiment. In contrast, “complete” simulations, which start from a singlet state on the hydrides and then calculate the evolving density matrix under exchange, give more insight into the spin system on the complex, but, with this “complete” approach, it is typically more tedious to achieve good agreement with experimental spectra. Since the SABRE field is currently undergoing a large expansion in available substrates and in applications, which range from chemical analysis to molecular imaging, it appears to be useful to have an inexpensive, low-field NMR approach to characterize hyperpolarization processes and hyperpolarized substances. Hyperpolarized, low-field rare spin spectroscopy may be used as a tool that gives detailed chemical information and insights into polarization transfer dynamics at the fields of the critical level-anti-crossings.

#### SUPPLEMENTARY MATERIAL

See the [supplementary material](#) for “complete” simulations of  $^{15}\text{N}$  and  $^{13}\text{C}$  acetonitrile isotopomers and “quick” simulations of  $^{15}\text{N}$ -pyridine and 3-fluoropyridine isotopomers (depicted in Fig. S1) with the corresponding spin labels. In addition, we provide all the  $J$ -coupling and chemical shift information values used in the simulations in tables, as well as an exemplary code for the “quick” and “complete” simulations.

#### AUTHOR'S CONTRIBUTIONS

M.S.R., S.A., and T.T. contributed equally to this work. S.L., M.S., A.K., and S.A. conducted the experiments in Aachen. Y.Y., M.S.R., and T.T. conducted the experiments in Boston. S.L. and T.T. designed simulation approaches for the NMR spectra. S.L. wrote the draft of the manuscript. All authors contributed revisions to the manuscript. B.B., M.S.R., S.A., and T.T. supervised the project.

#### ACKNOWLEDGMENTS

This research was supported by the National Institute of Biomedical Imaging and Bioengineering of the NIH under Grant No. R21EB025313. We also acknowledge support from the Oak Ridge Associated Universities, Ralph E. Powe Junior Faculty Enhancement Award, the North Carolina Biotechnology Center Translational Research Grant, as well as funding from the Mallinckrodt Foundation. Furthermore, the authors gratefully acknowledge technical support from Andreas Schwaitzer (ZEA-1) and financial support from Stefan van Waasen and Carsten Degenhardt (ZEA-2) of the Research Center Jülich.

## REFERENCES

- <sup>1</sup>K. Wüthrich, *Nat. Struct. Biol.* **8**, 923 (2001).
- <sup>2</sup>M. I. Choudhary, A. Rahman, and A. Wahab, *Solving Problems With NMR Spectroscopy*, 2nd ed. (Academic Press, Boston, 2016).
- <sup>3</sup>S. K. Sarkar, *NMR Spectroscopy and its Application to Biomedical Research* (Elsevier Science B.V., Amsterdam, 1996).
- <sup>4</sup>W. P. Aue, E. Bartholdi, and R. R. Ernst, *J. Chem. Phys.* **64**, 2229 (1976).
- <sup>5</sup>E. M. Purcell, H. C. Torrey, and R. V. Pound, *Phys. Rev.* **69**, 37 (1946).
- <sup>6</sup>P. T. Callaghan, *Principles of Nuclear Magnetic Resonance Microscopy* (Clarendon Oxford University Press, Oxford, 1994).
- <sup>7</sup>E. Danielli, J. Perlo, B. Blümich, and F. Casanova, *Angew. Chem., Int. Ed.* **49**, 4133 (2010).
- <sup>8</sup>S. Appelt, H. Kühn, F. W. Häsing, and B. Blümich, *Nat. Phys.* **2**, 105 (2006).
- <sup>9</sup>J. C. Allred, R. N. Lyman, T. W. Kornack, and M. V. Romalis, *Phys. Rev. Lett.* **89**, 130801 (2002).
- <sup>10</sup>J. B. Hövener, N. Schwaderlapp, T. Lickert, S. B. Duckett, R. E. Mewis, L. A. Highton, S. M. Kenny, G. G. Green, D. Leibfritz, J. G. Korvink, J. Hennig, and D. von Elverfeldt, *Nat. Commun.* **4**, 2946 (2013).
- <sup>11</sup>T. Theis, P. Ganssle, G. Kervern, S. Knappe, J. Kitching, M. P. Ledbetter, D. Budker, and A. Pines, *Nat. Phys.* **7**, 571 (2011).
- <sup>12</sup>J. Colell, P. Türschmann, S. Glöggler, P. Schleker, T. Theis, M. Ledbetter, D. Budker, A. Pines, B. Blümich, and S. Appelt, *Phys. Rev. Lett.* **110**, 137602 (2013).
- <sup>13</sup>M. P. Ledbetter, C. W. Crawford, A. Pines, D. E. Wemmer, S. Knappe, J. Kitching, and D. Budker, *J. Magn. Reson.* **199**, 25 (2009).
- <sup>14</sup>M. P. Ledbetter, T. Theis, J. W. Blanchard, H. Ring, P. Ganssle, S. Appelt, B. Blümich, A. Pines, and D. Budker, *Phys. Rev. Lett.* **107**, 107601 (2011).
- <sup>15</sup>J. N. Robinson, A. Coy, R. Dykstra, C. D. Eccles, M. W. Hunter, and P. T. Callaghan, *J. Magn. Reson.* **182**, 343 (2006).
- <sup>16</sup>T. Theis, M. P. Ledbetter, G. Kervern, J. W. Blanchard, P. J. Ganssle, M. C. Butler, H. D. Shin, D. Budker, and A. Pines, *J. Am. Chem. Soc.* **134**, 3987 (2012).
- <sup>17</sup>M. Suefke, A. Liebisch, B. Blümich, and S. Appelt, *Nat. Phys.* **11**, 767 (2015).
- <sup>18</sup>J. Anders, G. Chiamonte, P. SanGiorgio, and G. Boero, *J. Magn. Reson.* **201**, 239 (2009).
- <sup>19</sup>M. Abraham, M. A. H. McCausland, and F. N. H. Robinson, *Phys. Rev. Lett.* **2**, 449 (1959).
- <sup>20</sup>W. A. Barker, *Rev. Mod. Phys.* **34**, 173 (1962).
- <sup>21</sup>T. R. Carver and C. P. Slichter, *Phys. Rev.* **102**, 975 (1956).
- <sup>22</sup>T. G. Walker and W. Happer, *Rev. Mod. Phys.* **69**, 629 (1997).
- <sup>23</sup>G. Navon, Y. Q. Song, T. Room, S. Appelt, R. E. Taylor, and A. Pines, *Science* **271**, 1848 (1996).
- <sup>24</sup>S. Appelt, A. B. Baranga, C. J. Erickson, M. V. Romalis, A. R. Young, and W. Happer, *Phys. Rev. A* **58**, 1412 (1998).
- <sup>25</sup>R. G. Lawler, *J. Am. Chem. Soc.* **89**, 5519 (1967).
- <sup>26</sup>J. Bargon and H. Fischer, *Z. Naturforsch., A* **22**, 1556 (1967).
- <sup>27</sup>C. R. Bowers and D. P. Weitekamp, *J. Am. Chem. Soc.* **109**, 5541 (1987).
- <sup>28</sup>C. R. Bowers and D. P. Weitekamp, *Phys. Rev. Lett.* **57**, 2645 (1986).
- <sup>29</sup>R. W. Adams, J. A. Aguilar, K. D. Atkinson, M. J. Cowley, P. I. Elliott, S. B. Duckett, G. G. Green, I. G. Khazal, J. Lopez-Serrano, and D. C. Williamson, *Science* **323**, 1708 (2009).
- <sup>30</sup>E. B. Dücker, L. T. Kuhn, K. Münnemann, and C. Griesinger, *J. Magn. Reson.* **214**, 159 (2012).
- <sup>31</sup>H. Zeng, J. Xu, J. Gillen, M. T. McMahon, D. Artemov, J.-M. Tyburn, J. A. Lohman, R. E. Mewis, K. D. Atkinson, G. G. Green, S. B. Duckett, and P. C. van Zijl, *J. Magn. Reson.* **237**, 73 (2013).
- <sup>32</sup>R. A. Green, R. W. Adams, S. B. Duckett, R. E. Mewis, D. C. Williamson, and G. G. Green, *Prog. Nucl. Magn. Reson. Spectrosc.* **67**, 1 (2012).
- <sup>33</sup>M. J. Cowley, R. W. Adams, K. D. Atkinson, M. C. Cockett, S. B. Duckett, G. G. Green, J. A. Lohman, R. Kerssebaum, D. Kilgour, and R. E. Mewis, *J. Am. Chem. Soc.* **133**, 6134 (2011).
- <sup>34</sup>A. N. Pravdivtsev, A. V. Yurkovskaya, H.-M. Vieth, K. L. Ivanov, and R. Kaptein, *ChemPhysChem* **14**, 3327 (2013).
- <sup>35</sup>K. L. Ivanov, A. V. Yurkovskaya, and H.-M. Vieth, *J. Chem. Phys.* **128**, 154701 (2008).
- <sup>36</sup>L. Buljubasich, M. B. Franzoni, H. W. Spiess, and K. Münnemann, *J. Magn. Reson.* **219**, 33 (2012).
- <sup>37</sup>K. L. Ivanov, A. N. Pravdivtsev, A. V. Yurkovskaya, H.-M. Vieth, and R. Kaptein, *Prog. Nucl. Magn. Reson. Spectrosc.* **81**, 1 (2014).
- <sup>38</sup>M. L. Truong, T. Theis, A. M. Coffey, R. V. Shchepin, K. W. Waddell, F. Shi, B. M. Goodson, W. S. Warren, and E. Y. Chekmenev, *J. Phys. Chem. C* **119**, 8786 (2015).
- <sup>39</sup>J. F. Colell, A. W. Logan, Z. Zhou, R. V. Shchepin, D. A. Barskiy, G. X. Ortiz, Jr., Q. Wang, S. J. Malcolmson, E. Y. Chekmenev, W. S. Warren, and T. Theis, *J. Phys. Chem. C* **121**, 6626 (2017).
- <sup>40</sup>Q. Gong, A. Gordji-Nejad, B. Blümich, and S. Appelt, *Anal. Chem.* **82**, 7078 (2010).
- <sup>41</sup>D. A. Barskiy, K. V. Kovtunov, I. V. Koptuyg, P. He, K. A. Groome, Q. A. Best, F. Shi, B. M. Goodson, R. V. Shchepin, M. L. Truong, A. M. Coffey, K. W. Waddell, and E. Y. Chekmenev, *ChemPhysChem* **15**, 4100 (2014).
- <sup>42</sup>R. V. Shchepin, D. A. Barskiy, A. M. Coffey, M. A. Feldman, L. M. Kovtunova, V. I. Bukhtiyarov, K. V. Kovtunov, B. M. Goodson, I. V. Koptuyg, and E. Y. Chekmenev, *ChemistrySelect* **2**, 4478 (2017).
- <sup>43</sup>H. J. Hogben, M. Krzystyniak, G. T. Charnock, P. J. Hore, and I. Kuprov, *J. Magn. Reson.* **208**, 179 (2011).
- <sup>44</sup>M. Sarracanie, C. D. LaPierre, N. Salameh, D. E. J. Waddington, T. Witzel, and M. S. Rosen, *Sci. Rep.* **5**, 15177 (2015).
- <sup>45</sup>T. Theis, M. L. Truong, A. M. Coffey, R. V. Shchepin, K. W. Waddell, F. Shi, B. M. Goodson, W. S. Warren, and E. Y. Chekmenev, *J. Am. Chem. Soc.* **137**, 1404 (2015).
- <sup>46</sup>R. L. Lichter and J. D. Roberts, *J. Am. Chem. Soc.* **93**, 5218 (1971).
- <sup>47</sup>W. A. Thomas and G. E. Griffin, *Org. Magn. Reson.* **2**, 503 (1970).
- <sup>48</sup>S. Lehmkuhl, M. Emondts, L. Schubert, P. Spanning, J. Klankermayer, B. Blümich, and P. P. M. Schleker, *ChemPhysChem* **18**, 2426 (2017).
- <sup>49</sup>S. Lehmkuhl, M. Wiese, L. Schubert, M. Held, M. Küppers, M. Wessling, and B. Blümich, *J. Magn. Reson.* **291**, 8 (2018).
- <sup>50</sup>D. A. Barskiy, A. N. Pravdivtsev, K. L. Ivanov, K. V. Kovtunov, and I. V. Koptuyg, *Phys. Chem. Chem. Phys.* **18**, 89 (2016).
- <sup>51</sup>P. J. Rayner, P. Norcott, K. M. Appleby, W. Iali, R. O. John, S. J. Hart, A. C. Whitwood, and S. B. Duckett, *Nat. Commun.* **9**, 4251 (2018).
- <sup>52</sup>W. Iali, S. S. Roy, B. J. Tickner, F. Ahwal, A. J. Kennerley, and S. B. Duckett, *Angew. Chem., Int. Ed.* **58**, 10271 (2019).
- <sup>53</sup>R. E. Mewis, R. A. Green, M. C. Cockett, M. J. Cowley, S. B. Duckett, G. G. Green, R. O. John, P. J. Rayner, and D. C. Williamson, *J. Phys. Chem. B* **119**, 1416 (2015).
- <sup>54</sup>M. Suefke, S. Lehmkuhl, A. Liebisch, B. Blümich, and S. Appelt, *Nat. Phys.* **13**, 568 (2017).
- <sup>55</sup>S. Knecht, S. Hadjiali, D. A. Barskiy, A. Pines, G. Sauer, A. S. Kiryutin, K. L. Ivanov, A. V. Yurkovskaya, and G. Buntkowsky, *J. Phys. Chem. C* **123**, 16288 (2019).
- <sup>56</sup>R. V. Shchepin, B. M. Goodson, T. Theis, W. S. Warren, and E. Y. Chekmenev, *ChemPhysChem* **18**, 1961 (2017).
- <sup>57</sup>K. Buckenmaier, K. Scheffler, M. Plaumann, P. Fehling, J. Bernarding, M. Rudolph, C. Back, D. Koelle, R. Kleiner, J. B. Hövener, and A. N. Pravdivtsev, *ChemPhysChem* **20**, 2823 (2019).